Case Studies in Thermal Engineering 50 (2023) 103438

Contents lists available at ScienceDirect

Case Studies in Thermal Engineering

journal homepage: www.elsevier.com/locate/csite

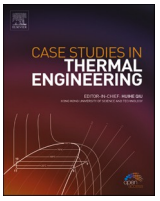

Optimizing fluid parameters of heat transfer and velocity of aluminum oxide nanoparticles and SWCNT passing through blades using RSM statistical method

As'ad Alizadeh [a], Bashar Mahmood Ali [b], Kadhim Abbas Jabbar [c], Pooya Pasha [d,*], Ahmed hasoon [e], Mahmoud Shamsborhan [f]

[a] Department of Civil Engineering, College of Engineering, Cihan University-Erbil, Erbil, Iraq
[b] Department of Construction Engineering & Project Management, Al-Noor University College, Nineveh, Iraq
[c] National University of Science and Technology, Dhi Qar, Iraq
[d] Department of Mechanical Engineering Mazandaran University of Science and Technology, Babol, Iran
[e] Engineering Technical College, Al-Farahidi University, Iraq
[f] Department of Mechanical Engineering, College of Engineering University of Zakho, Zakho, Iraq

ARTICLE INFO

Handling Editor: Huihe Qiu

Keywords:
Optimizing fluid parameters
Finite element method
SWCNT effects
Thread stretching sheet
RSM statistical method

ABSTRACT

This paper explores how the temperature and velocity change in a specific direction and the rotational velocity when nanofluids flow through triangular, rectangular, and chamfer baffles. The novelty of this article is to study and investigate the thermal and fluidic parameters of the velocity gradient and heat transferred between aluminum oxide and SWCNT nanofluids on the tensile surface. This study aims to increase the heat transfer coefficient by installing blades with different shapes. The Finite Element Method is chosen to solve the main equations. This paper utilized the RSM method to optimize the velocity of nanofluid and heat transfer as it passes through the stretching sheet. The main goal of this study mentioned in the article is to explore the impact of various vane shapes installed on the outer surface of a stretched sheet. To summarize, after analyzing the flow of SWCNT and Al_2O_3 nanofluids on various baffles and blades, it was found that the temperature of SWCNT nanofluid around the baffles was higher compared to the temperature of Al_2O_3 nanofluids. According to the results from the graphs of how fast something is turning and the factors that transfer heat in the software called Design-Expert, the best improvement happened when the velocity and temperature of the small particles in the liquid were at u = 1.12, and T = 20.18 and the turning velocity was N = 137.29.

Nomenclature

κ	Vortex viscosity(l/t)
T_w	Wall temperature (F°)
F	Stream function (kg/ms)
Φ	Ferrofluid volume fraction (nm)
σ_{nf}	Electric conductivity of Ferrofluid(S/m)

* Corresponding author.
E-mail address: Poooyaenginer@gmail.com (P. Pasha).

https://doi.org/10.1016/j.csite.2023.103438
Received 8 July 2023; Received in revised form 26 August 2023; Accepted 31 August 2023
Available online 9 September 2023

p	Pressure (pascal)
S	Ferrofluid particle (nm)
nf	Ferrofluid (nm)
W	Situation at wall (mm)
∞	Situation at infinity
$Cp_{n,f}$	Ferrofluid heat capacity (J/K)
$_{k}$	Micro-rotation variable
$_{\gamma nf}$	Spin-gradient viscosity (Pa·s)
f_0	Petukhov's correction factor W/(m^{2}K)
I	Body couple of mass parameter (kg)
j	Inertia density (kg. m^2)
μ_f	Base fluid dynamic viscosity (Pa·s)
T∞	Ambient temperature(F°)
N	Rotation vector (Θ)
k_{nf}	Ferrofluid thermal conductivity (Wm^{-1}K^{-1})
k_f	Fluid thermal conductivity(Wm^{-1}K^{-1})
f	Base fluid (gal/sk)
ρfMeasure fluid density (kg/m^3)	ρs Measure fluid density (kg/m^3)
ρsFerrofluid density (kg/m^3)	
qr	Radiation heat flux (W/m^2)
R	Radiation variable (pCi)
φ	Spin gradient viscosity(Pa·s)
α	Stretching/shrinking variable
σ_s	Ferroparticles electric conductivity(S/m)
$\sigma*$	Stefan-Boltzmann parameter (W/(m^2 x K^4)σTension parameter (N)
u	x-ingredient of velocity (m/s)
v	y– ingredient of velocity (m/s)
μ_{nf}	Ferrofluid viscosity(Pa·s)

1. Introduction

A thin sheet was stretched out with some fins that pointed up. They envisioned a continuous movement of a unique type of fluid that deviates from the typical behavior exhibited by conventional fluids. A ferrofluid is a liquid with small pieces of iron, magnetite, or cobalt floating in it. Ferrofluids are a mixture of small iron pieces that can move because they are in oil. This oil is usually kerosene, and a particular ingredient is added to stop parts from sticking together. Ferrofluids help stop moving parts from making too much noise in computers, motors, and speakers. Scientists explored how to use math methods to understand how fluids with unique properties move through small spaces and transfer heat in materials that allow substances to pass through them [1]. The importance of nanomaterials lies in their ability to revolutionize various industries, including electronics, energy, and medicine, by offering enhanced performance attributes. Nanomaterials are characterized by their distinct structures and properties, which greatly differ from those of larger bulk materials, owing to their small size. Typically ranging between 1 and 100 nm, these materials exhibit exceptional physical, chemical, and biological attributes that set them apart [2–8]. Following two critical scientific rules, this study looked at how twisted porous ribs in a tiny channel affect how heat and energy move around. The outcome proves that adding porous ribs makes the area narrower and the flow stronger [9]. The study used math to determine how many iron oxide nanoparticles are in a triangle-shaped container with a wavy hot wall. According to Ref. [10], as the undulation number increases, the Nusselt number decreases, while an increase in the Rayleigh number leads to an increase in the Nusselt number. This research wants to see how putting magnets near water mixed with tiny tubes and iron affects their movement [11]. This study examines how heat and fluid behavior change in a small channel with bumps on its walls. The fluid has tiny particles in it that are magnetic. The researchers use different methods to understand what happens when the fluid flows with and without heat. This research looks at how different facts are related to each other. The study shows that factors like how much space is empty in material and numbers called Reynolds and Hartmann numbers make the transfer of heat better [12]. They studied how a special liquid called "nanofluid" flows over a sheet that is getting smaller. They also looked at how a magnet on the side effects the flow. This work is about a new way to model a type of liquid with tiny particles called a hybrid nanofluid. The model uses a method that looks at the masses of the liquid and the particles to determine how it behaves. This is something new and different [13]. Dinarvand and his colleagues studied the flow of a mix of small particles and liquid that can't be compressed between two parallel sheets that move back and forth. They used math to understand how a magnetic field and changing heat affect this flow [14]. This study examined how fluids with tiny particles (nanofluids) flow warmed up and moved over a wedge. The study used computer simulations to see what happens. The small particles used in the research are called magnetite and graphene oxide. They come in different shapes, like spheres, bricks, cylinders, platelets, and disks. They are mixed with pure water [15]. Mohammad Izady et al. [16] studied how a mixture of Fe2O3, CuO, and water flows over a wedge that changes shape using math and physics. They also looked at how radiation and magnetism affect the flow. Emad Ismat Ghandourah et al. [17] tested a new way to make fresh water using the sun. They used a machine with two slopes for collecting water, and we painted it with special chemicals to

Table 1
Properties of water and Al_2O_3 and SWCNT nanoparticles at 25°.

	ρ (kg/m^3)	K (w/m.k)	C_p (j/kg.k)	σ
H_2O	997	0.613	4179	0.05
Al_2O_3	3970	25	765	10^{-12}
SWCNT	2600	6600	425	0.00002

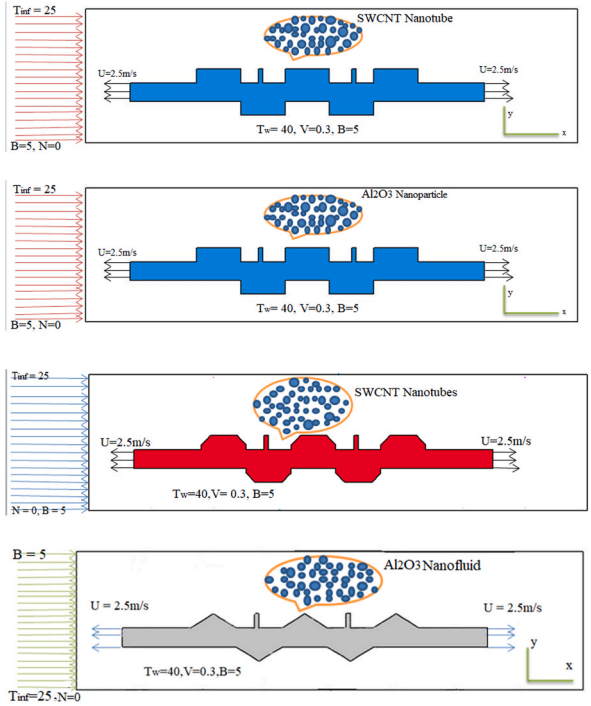

Fig. 1. The geometry of the problem comparing different nanoparticles passing through a Triangular, rectangular and chamfer baffles.

make it work better. This paper [18] looks at how plates made of two different materials behave when they are bent or topple over, and if there are any small holes in them. The new theory says that the BFG plates have no sideways pressure at two of their exposed sides. Response Surface Methodology (RSM) is a way to use math to make sure we do things the best way possible. RSM is a method that uses the ideas of how to plan experiments, also known as DOE [19–21]. This study [22] helps us understand how friction affects heated and slanted surfaces when water or other substances flow over them. Scientists studied how Hall and ion slip effects impact the movement of fluids through a porous material rotating and experiencing unsteady magnetic fields [23]. Scientists researched how chemicals react on a moving vertical plate with heat and fluid motion [24,25]. This work transforms the nonlinear PDE into a two-point limit problem with similarity and t-variables [26,27]. Researchers examined how liquid moves on a spinning, flexible disk with heat transfer [28]. The new initiative used in this study includes three essential and fundamental items. First, the parameters of SWCNT and Al2O3 nanoparticles that pass through different fins and blades are investigated, and their results are compared. Also, the velocity and temperature parameters are processed with the VIM mathematical analysis method. Finally, by addressing the statistical way of RSM, we will optimize the placement of the blades at the distance of the tension plane to reach the best velocity and temperature at those points. Response Surface Methodology (RSM) is a set of methods that use numbers and statistics to make experimental data fit into mathematical models called polynomials. Specific goals are now being pursued in earnest, the most important of which is to improve the process by finding optimal inputs, eliminating process problems and weaknesses and stabilizing them [29–34]. Saeed Dinarvand and his colleagues [35] wrote this. The researchers studied how a special mixture of MgO–Ag nanoparticles and water moves around a thin needle that is moving. They looked at two possible explanations for this movement. The researchers studied the flow of a type of liquid with tiny particles and magnets. They looked at how the flow changed when there was heat added or removed, different shapes of the particles, and a magnetic field at an angle [36,37]. The main goal of this study mentioned in the article is to explore the impact of various vane shapes installed on the outer surface of a stretched sheet. The researchers are particularly interested in understanding the amount of heat that can be transferred from the sheet's surface to nanofluids, and which specific nanofluids are more compatible for the screen cooling process. By investigating these factors, the study aims to provide insights into optimizing the cooling efficiency of screens. The RSM statistical method was utilized in this study to optimize the fluid values of temperature and speed. The findings demonstrated the specific points on the plate and the type of blades that result in higher magnitudes of changes in speed and

temperature gradients. This analysis helps to identify the most effective configurations for achieving desired performance outcomes. The utilization of two SWCNT and Al_2O_3 nanofluids in this study was due to their superior conduction heat transfer coefficient and ability to transfer heat efficiently at a constant pressure. The novelty of this article is to study and investigate the thermal and fluidic parameters of the velocity gradient and heat transferred between aluminum oxide and SWCNT nanofluids on the tensile surface. This study aims to increase the heat transfer coefficient by installing blades with different shapes (see Table 1).

2. Problem definition

Think about small particles moving through a special liquid that contains two things called SWCNT and Al_2O_3. These particles flow past the thin pieces of material on a sheet that's being pulled tight. We use three different types of baffles on the surfaces: triangular, rectangular, and chamfer. The magnetic things around the baffles and blades are essential. The small liquid flows at 25°, doesn't spin from one direction, and goes through the baffles and surface (Fig. 1). The surface is hot at 40°, and it has been pulled in one direction by velocity (UW(x) = ax, a>0). The object moves at a velocity of 2.5 m per second to the side (x-direction) and 0.2 m per second up or down (y-direction); the volume concentration of nanofluids is between 0.03 and 0.04. In this article, we study how the magnetic force affects the surface. This article uses the finite element method to solve a problem.

This article uses the finite element method to solve a problem. These are the equations that guide how Ferrofluid works [28]:

$$\frac{D\rho_{nf}}{dt}=\left(u^*.\frac{d\rho_{nf}}{dx}+v^*.\frac{d\rho_{nf}}{dy}+w^*.\frac{d\rho_{nf}}{dz}\right).\left(\rho_{nf}.\frac{du^*}{dx}+\rho_{nf}.\frac{dv^*}{dy}+\rho_{nf}.\frac{dw^*}{dz}\right) \tag{1}$$

$$\rho_{nf}.\left(\frac{DV^*}{dt}\right)=-\nabla_p+\left(2.\mu_{nf}+\aleph\right)\nabla\left(\rho_{nf}.\frac{du^*}{dx}+\rho_{nf}.\frac{dv^*}{dy}+\rho_{nf}.\frac{dw^*}{dz}\right)-\left(\mu_{nf}+\aleph\right)\nabla.\left(\rho_{nf}.\frac{du^*}{dx}+\rho_{nf}.\frac{dv^*}{dy}+\rho_{nf}.\frac{dw^*}{dz}\right)+\aleph(\nabla.N^*)j.B^*+\rho_{nf}.g \tag{2}$$

$$j.B=-\sigma_{nf}.B_0^{*2}.u^* \tag{3}$$

$$j.B=-\sigma_{nf}.B_0^{*2}.v^* \tag{4}$$

$$j.B=-\sigma_{nf}.B_0^{*2}.w^* \tag{5}$$

$$N^*=-\delta.\left(\frac{du^*}{dy}+\frac{dv^*}{dz}+\frac{dw^*}{dx}\right) \tag{6}$$

Equation (1) is a way to measure how much of it there is. Equation number 2 shows how momentum changes. Hussanan et al. came up with a force that affects the body, called j. BIn equations (3)–(5), N* means how fast something is spinning (6). We put some equations into other equations to figure out how things move in different directions [28]:

$$\begin{aligned}\rho_{nf}.\left(\frac{Du^*}{dt}\right)=&-\frac{dp^*}{dx}+\left(2.\mu_{nf}+\aleph\right)\nabla\left(\rho_{nf}.\frac{du^*}{dx}+\rho_{nf}.\frac{dv^*}{dy}+\rho_{nf}.\frac{dw^*}{dz}\right)-\left(\mu_{nf}+\aleph\right)\nabla.\left(\rho_{nf}.\frac{du^*}{dx}+\rho_{nf}.\frac{dv^*}{dy}+\rho_{nf}.\frac{dw^*}{dz}\right)\\&+\aleph\left(\nabla.-\delta.\left(\frac{du^*}{dy}+\frac{dv^*}{dz}+\frac{dw^*}{dx}\right)\right)-\sigma_{nf}.B_0^{*2}u^*+\rho_{nf}.g\end{aligned} \tag{7}$$

$$\begin{aligned}\rho_{nf}.\left(\frac{Dv^*}{dt}\right)=&-\frac{dp^*}{dy}+\left(2.\mu_{nf}+\aleph\right)\nabla.\left(\rho_{nf}.\frac{du^*}{dx}+\rho_{nf}.\frac{dv^*}{dy}+\rho_{nf}.\frac{dw^*}{dz}\right)-\left(\mu_{nf}+\aleph\right)\nabla.\left(\rho_{nf}.\frac{du^*}{dx}+\rho_{nf}.\frac{dv^*}{dy}+\rho_{nf}.\frac{dw^*}{dz}\right)\\&+\aleph\left(\nabla.-\delta.\left(\frac{du^*}{dy}+\frac{dv^*}{dz}+\frac{dw^*}{dx}\right)\right)-\sigma_{nf}.B_0^{*2}.v^*+\rho_{nf}.g\end{aligned} \tag{8}$$

$$\begin{aligned}\rho_{nf}.\left(\frac{Dw^*}{dt}\right)=&-\frac{dp^*}{dz}+\left(2.\mu_{nf}+\aleph\right)\nabla\left(\rho_{nf}.\frac{du^*}{dx}+\rho_{nf}.\frac{dv^*}{dy}+\rho_{nf}.\frac{dw^*}{dz}\right)-\left(\mu_{nf}+\aleph\right)\nabla.\left(\rho_{nf}.\frac{du^*}{dx}+\rho_{nf}.\frac{dv^*}{dy}+\rho_{nf}.\frac{dw^*}{dz}\right)\\&+\aleph\left(\nabla.-\delta.\left(\frac{du^*}{dy}+\frac{dv^*}{dz}+\frac{dw^*}{dx}\right)\right)-\sigma_{nf}.B_0^{*2}.w^*+\rho_{nf}.g\end{aligned} \tag{9}$$

The energy equation is presumed in the following section [28]:

$$\begin{aligned}\rho_{nf}j.\left(\frac{dN^*}{dt}\right)=&\left(\varphi+\lambda+Y_{nf}\right)\nabla.\left(\rho_{nf}.-\delta.\left(\frac{du^*}{dy}+\frac{dv^*}{dz}+\frac{dw^*}{dx}\right)\right)-Y_{nf}.\nabla.\left(\nabla.-\delta.\left(\frac{du^*}{dy}+\frac{dv^*}{dz}+\frac{dw^*}{dx}\right)\right)\\&+\aleph.\left(\rho_{nf}.\frac{du^*}{dx}+\rho_{nf}.\frac{dV^*}{dy}+\rho_{nf}.\frac{dw^*}{dz}\right)-2.\aleph.\left(-\delta.\left(\frac{du^*}{dy}+\frac{dv^*}{dz}+\frac{dw^*}{dx}\right)\right)+\rho_{nf}.I\end{aligned} \tag{10}$$

Brinkman [22], Bourantas, and Loukopoulos [23] explained how effective density, dynamic viscosity, and spin gradient viscosity work in a previous study.

$$\rho_{nf}=\rho_f-\varphi.\rho_f+\varphi.\rho_s \tag{11}$$

$$\mu_{nf} = \frac{\mu_f}{(1-\varphi)^{2.5}} \tag{12}$$

$$Y_{nf} = \left(\frac{\mu_f}{(1-\varphi)^{2.5}} + \aleph 2\right) j \tag{13}$$

Also, flow cannot be compressed when no outside forces are acting on it. The math problems will take a lot of work to solve.

$$\rho_{nf.}\left(\frac{dv^*}{dt} + \left(\rho.\frac{du^*}{dx} + \rho.\frac{dV^*}{dy} + \rho.\frac{dw^*}{dz}\right).v^*\right) = \left(\mu_{nf} + \aleph\right)\nabla^2.v^* + \aleph.(\nabla.N^*) + -\sigma_{nf}.B_0^{*2}.v^* \tag{14}$$

$$\rho_{nf}.j.\left(\frac{dN^*}{dt} + (N^*.\nabla).N^*\right) = Y_{nf}.\nabla^2.N^* + \aleph.\left(\rho.\frac{du^*}{dx} + \rho.\frac{dV^*}{dy} + \rho.\frac{dw^*}{dz}\right)2.\aleph.N^* \tag{15}$$

The Ferro fluid electric conductivity represents [25]:

$$\sigma_{nf} = \left[\sigma_f + \sigma_f.\frac{\mathbf{3}.\boldsymbol{\sigma}.\varnothing - \mathbf{3}.\varnothing}{(\boldsymbol{\sigma}+\mathbf{2}) - (\boldsymbol{\sigma}.\varnothing - \varnothing)}\right] \tag{16}$$

And the governing equations go to:

$$\rho_{nf}\left(u^*.\frac{du^*}{dx} + v.\frac{du^*}{dy}\right) = \left(\mu_{nf} + \aleph\right).\frac{d^2u^*}{dy^2} + \aleph.\frac{dN^*}{dy} - \sigma_{nf}.B_0^{*2}.u^* \tag{17}$$

$$\rho_{nf}j\left(u^*.\frac{dN^*}{dx} + v^*.\frac{dN^*}{dy}\right) = Y_{nf}.\frac{d^2N^*}{dy^2} - \aleph.\left(2.N^* + \frac{du^*}{dy}\right) \tag{18}$$

Vajravelu [26] and Khan et al. [27] studied how well materials can hold heat and transfer it.

$$C_{p,nf} = \frac{C_p)s + (1-\varnothing)\rho_f.Cp_f}{\rho_f - \varphi.\rho_f + \varphi.\rho_s} \tag{19}$$

$$\frac{k_{nf}^*}{k_f^*} = \frac{2.k_1^* + k_p^* - 2.\varnothing.\left(k_f^* - k_p^*\right)(1+\eta)^3}{2.k_1^* + k_p^* + \varnothing.\left(k_f^* - k_p^*\right)(1+\eta)^3} \tag{20}$$

The following process examines the energy equation:

$$u^*.\frac{dT^*}{dx} + v^*.\frac{dT^*}{dy} = \frac{2.k_1^* + k_p^* - 2.\varnothing.\left(k_f^* - k_p^*\right).(1+\eta)^3}{\frac{C_p)s+(1-\varnothing).\rho_f.Cp_f}{\rho_f-\varphi.\rho_f+\varphi.\rho_s}}\ \frac{d^2T^*}{dy^2} - \frac{dq_r}{dy} \tag{21}$$

According to Rosseland's approximation, it is given by:

$$u^*.\frac{dT^*}{dx} + v^*.\frac{dT^*}{dy} = \frac{1}{\frac{C_p)s+(1-\varnothing)\rho_f.Cp_f}{\rho_f-\varphi.\rho_f+\varphi.\rho_s}}\left(\frac{C_p)s + (1-\varnothing)\rho_f.Cp_f}{\rho_f - \varphi.\rho_f + \varphi.\rho_s} + \frac{16.\sigma^*.T_\infty^{*3}}{3.k^*}\right)\ \frac{d^2T^*}{dy^2} \tag{22}$$

The boundary equations are [28]:

$$u^* = a.u_w(x), v^* = v_w^*, at\ \ y = 0 \ll \gg u^* \to 0\ \ at \quad y \to \infty \tag{23}$$

$$N^* = -\delta.\frac{du^*}{dy} \quad at \quad y = 0 \ll \gg N^* \leftrightarrow 0\ \ at \quad y \to \infty \tag{24}$$

$$T^* = T_w^*, at \quad y = 0 \ll \gg T^* \leftrightarrow T_w^* \quad at \quad y \to \infty \tag{25}$$

Velocity components in x and y directions, u and v, are adopted. Suction and injection are shown by using numbers to describe how fast the mass moves on the surface. Positive numbers mean suction, while negative numbers mean injection. Angular velocity measures how fast something is spinning and is usually written as N*. μ means how sticky a fluid is, and δ is a number between 0 and 1 that stays the same. When the number is 0, it means the microelement is identified. If the value of δ is 1/2, then the amount of small substances in a sample was found to be low [28].

$$\eta = y\sqrt{\frac{a}{\vartheta_f}}, u = axF^{'}(\eta), v = -\sqrt{\alpha\vartheta_f}F(\eta), N = ax\sqrt{\frac{a}{\vartheta_f}}G(\eta), \theta(\eta) = \frac{T - T_\infty}{T_w - T_\infty} \tag{26}$$

We can put numbers into the formula to solve the equations. In numbers 14, 15, and 21, we have [28]:

$$\left(\frac{1}{(1-\varnothing)^{2.5}}+k\right)F^{'''}(\eta)+\left(1-\varnothing+\varnothing\frac{\rho_s}{\rho_f}\right)F(\eta)F^{''}(\eta)-\left(1-\varnothing+\varnothing\frac{\rho_s}{\rho_f}\right)F^{'2}(\eta)-M\left(1+\frac{3(\sigma-1)\varnothing}{\sigma+2-(\sigma-1)\varnothing}\right)F^{'}(\eta)+kG^{'}(\eta)=0 \quad (27)$$

$$\left(\frac{1}{(1-\varnothing)^{2.5}}+\frac{k}{2}\right)G^{''}(\eta)+\left(1-\varnothing+\varnothing\frac{\rho_s}{\rho_f}\right)F(\eta)G^{'}(\eta)-\left(1-\varnothing+\varnothing\frac{\rho_s}{\rho_f}\right)F^{'}(\eta)G(\eta)-k(2G(\eta)+F^{''}(\eta))=0 \quad (28)$$

$$\frac{1}{Pr}\left(\frac{k_s+2k_f-2\varnothing(k_f-k_s)}{k_s+2k_f+\varnothing(k_f-k_s)}+R\right)\theta^{''}(\eta)+\left(1-\varnothing+\frac{C_p)s}{C_p)f}\right)F(\eta)\theta^{'}(\eta)=0 \quad (29)$$

And here the new boundary conditions:

$$F(\eta)=S,F^{'}(\eta)=\alpha,G(\eta)=-\delta F^{''}(\eta),\theta(\eta)=1,at\ \eta=0 \quad (30)$$

$$F^{'}(\eta)\leftrightarrow 0,G(\eta)\leftrightarrow 0,\theta(\eta)\to 0 \quad at\ \ \eta\to\infty \quad (31)$$

3. Computer simulation methodology

3.1. Finite element theory (FEM) and variation iteration theory (VIM)

The finite element method is a beneficial way to solve problems in fluid, heat, and math fields. It can help with linear and non-linear equations. FEM is a common way to solve boundary problems involving two or three space factors. Most of the time, it is impossible to solve Partial Differential Equations using mathematical methods for various shapes and issues. Instead, we can estimate these equations by breaking them into smaller parts and solving them with math on a computer. That means our answers are different from the solutions for those complicated math problems. The FEM is a way to simplify complex spaces. It divides them into smaller pieces called finite elements. These pieces can be described using simple equations. The simple idea behind this method comes from the laws of motion, conservation of mass and energy, and the laws of thermodynamics, as discovered by Sir Isaac Newton. Finally, the finite element method for a boundary problem is defined using a system of logarithmic conditions.

3.1.1. VIM theory

The symbol Ω represents the frequency of an oscillator. To get different sentences of u, use a formula with a multiplier λ:

$$u^{*^{'}}+\Omega^2=F(u^*)$$

$$F(u^*)=\Omega^2u^*-\mathrm{f}(u^*) \quad (26)$$

Given the boundary equations:

$$u^{*^{'}}=0,$$

$$u^*(0)=\mathrm{A} \quad (27)$$

And the first functions:

$$u_0^*(\mathrm{t})=\mathrm{A}\cos\Omega \quad (28)$$

$$\int_0^{\mathrm{T}}\cos\Omega\mathrm{t}\left[\Omega^2u_0^*-\mathrm{f}\left(u_0^*\right)\right]\mathrm{dt}=0 \quad (29)$$

We get the λ number by dividing one part of the equation by another. Different ways of defining sentences are used for a more accurate answer about their number.

$$u_{n+1}^*(t)=u_n^*(t)+\int_0^{\mathrm{t}}\lambda\left\{\frac{\mathrm{d}^2u_n^*}{\mathrm{d}\eta^2}+\Omega^2u_n^*(\eta)-\mathrm{F}_n\right\}\mathrm{d}\eta \quad (30)$$

Where λ is the Lagrange coefficient and F_n is considered various restricted:

3.2. Response Surface Methodology, (RSM) technique

Response Surface Methodology (RSM) is a set of methods that use numbers and statistics to make experimental data fit into mathematical models called polynomials. RSM is a study method used in experiments and science. With RSM, scientists design experiments to learn about interactions, second-degree effects, and the shape of the result they are studying. Specific goals are now being pursued in earnest, the most important of which is to improve the process by finding optimal inputs, eliminating process problems and weaknesses, and stabilizing them.

To give more details about the meshes, Figure (2) shows graphs with two dimensions as part of a test for grid independence. According to the speed and thermal process graphs, it can be concluded that as the heat changes more and more, the number of meshes

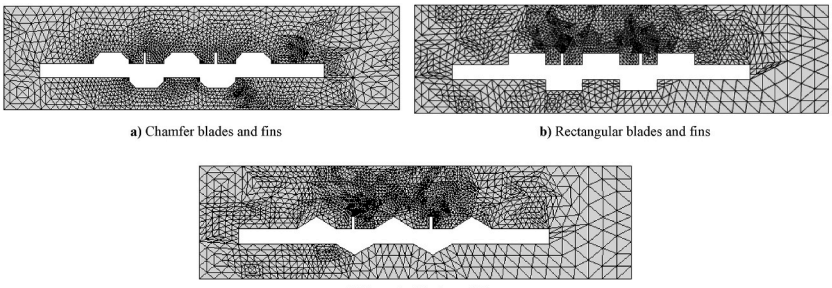

a) Chamfer blades and fins

b) Rectangular blades and fins

c) Triangular blades and fins

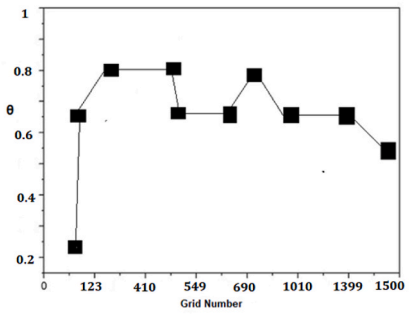

d) Grid independent test for temperature

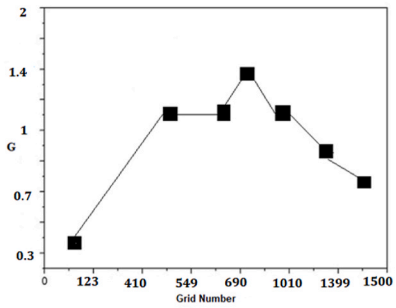

e) Grid independent test for velocity

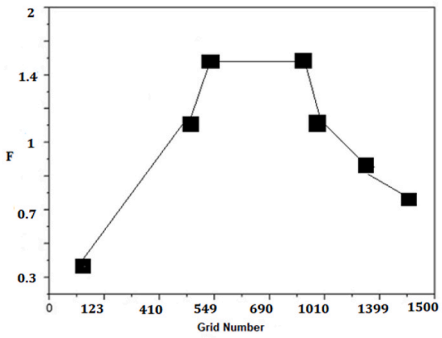

F) Grid independent test for stream function.

Fig. 2. Comparison of mesh geometry for stretching sheets and Grid independent test for temperature and velocity around the stretching sheet.

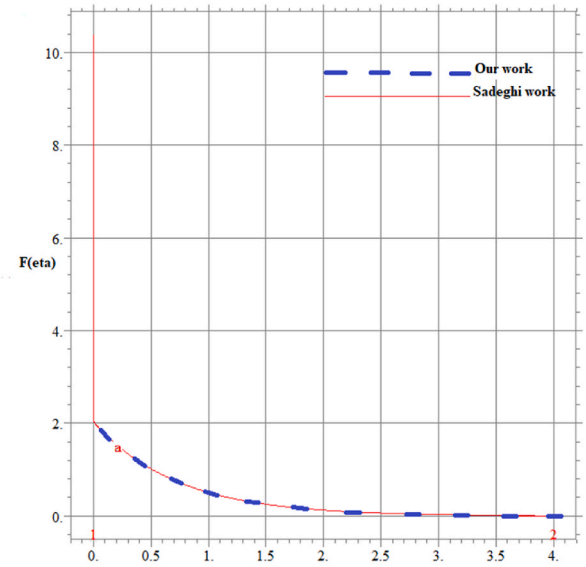

(a)

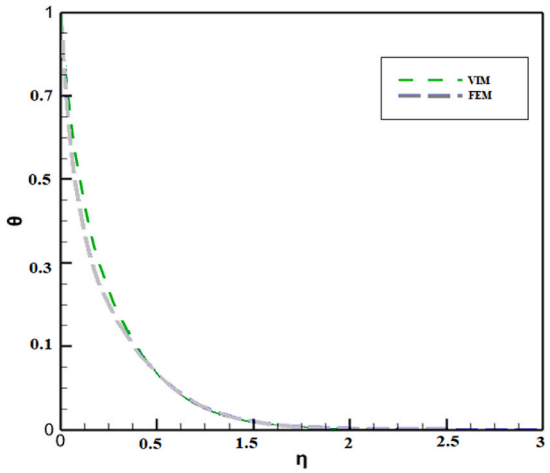

(b)

Fig. 3. (a)Schematic of the comparison of the present study with Sadeghi work [23] for velocity component at K = 10, δ = 0.6, φ = 0.04, and (b) Schematic of the comparison of the Variation iteration study with FEM method for temperature component at K = 10, δ = 0.6, φ = 0.04.

Table 2
Schematic of the comparison of the present study with Sadeghi work [23] in table format for velocity component at K = 10, δ = 0.6, φ = 0.04.

	$\eta = 0.0$	$\eta = 1$	$\eta = 1.5$	$\eta = 2$	$\eta = 2.5$	$\eta = 4$
Our work	2	0.73	0.61	0.52	0.36	0.01
Sadighi [23]	2	0.78	0.60	0.51	0.36	0.01

on the surfaces and around the fins fluid increases, and the quality of meshes becomes better. According to Fig. 2, the largest meshes are located at the edges because the Nanofluidic flow properties of temperature and velocity change around the baffles.

3.3. Validation

Based on Figure (3a) and Table 2, the statistical data of the present study has been evaluated and reviewed with the article of Dr. Sadeghi and his colleagues [23]. The number of miscalculations in the current work needs to be revised compared to Sadeghi's article. Computational data in the same case intervals in both articles were obtained entirely convergently. First, in Figure (3b), a comparison of the calculated results of the heat transfer parameter for two numerical methods has been made. In the range of the plane stretched from two sides, for the temperature parameter, the calculations made by both methods are close to each other and follow similar

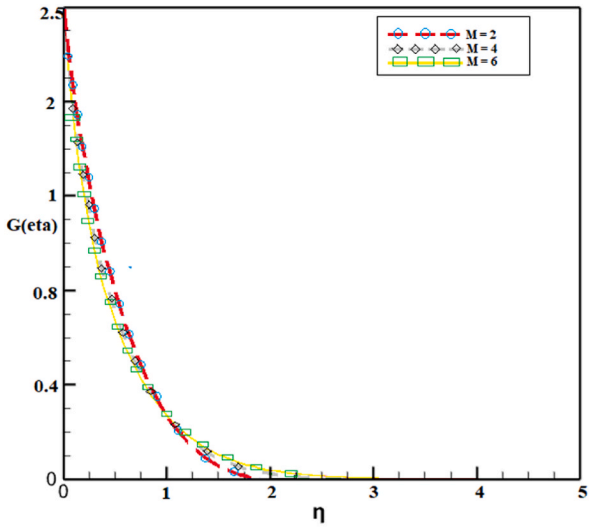

(a)

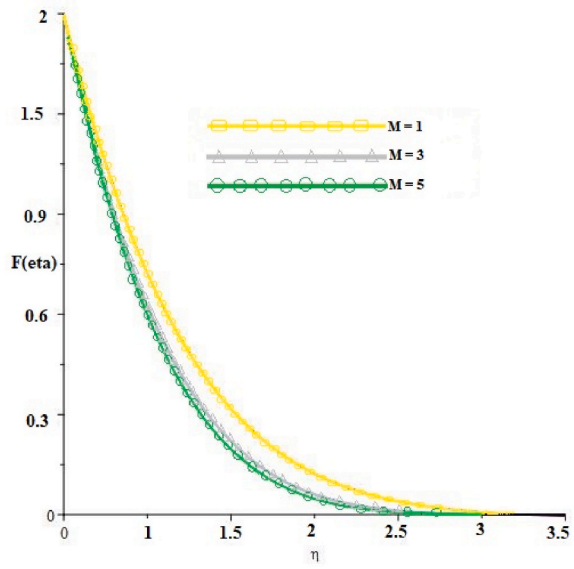

(b)

Fig. 4. Schematic of the graphical changes of the (a) velocity parameter and (b) stream parameter with respect to different values of M in the VIM technique.

results. This shows the correctness of validating the VIM numerical analytical course.

3.4. Usage of variation iteration method

Based on the Variation iteration strategy, the straight parts of the coupling conditions are composed as follows:

$$\frac{d^3}{d\eta^3}f_0(\eta) = 0 \tag{31}$$

$$\frac{d^2}{d\eta^2}\theta_0(\eta) = 0 \tag{32}$$

$$\frac{d^2}{d\eta^2}G_0(\eta) = 0 \tag{33}$$

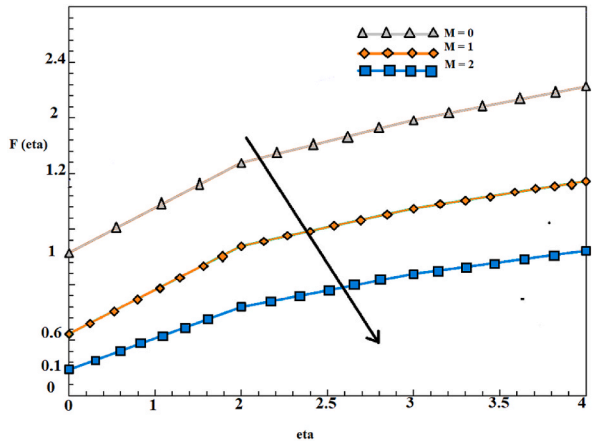

Fig. 5. Schematic of the graphical changes of the stream parameter with respect to different values of injection and stretching in the VIM technique for $S > 0$, $\alpha > 0$.

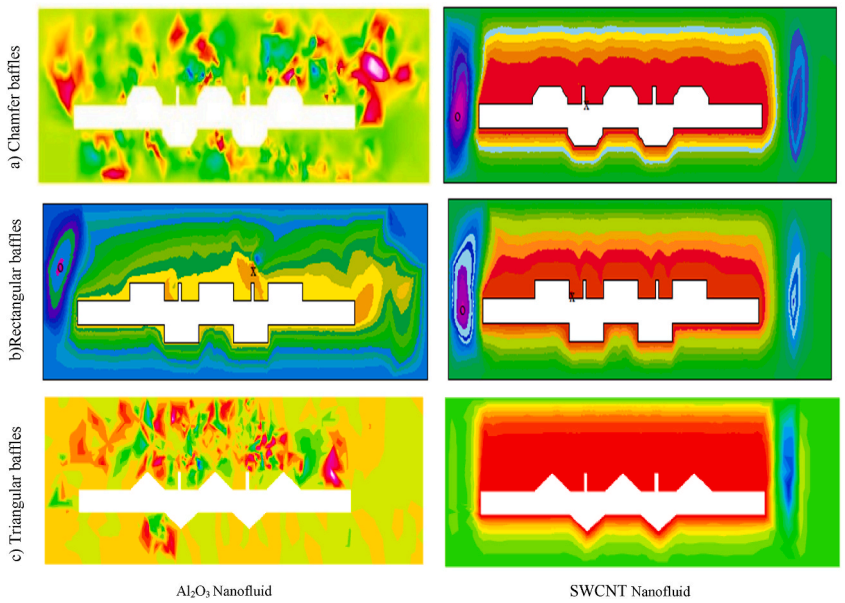

Fig. 6. Spreading heat flux from different types of blades with different geometries with two nanofluids SWCNT and Al_2O_3.

In this case, the boundary condition for the linear part is expressed as:

$$F(\eta) = S, F'(\eta) = \alpha, G(\eta) = -\delta F''(\eta), \theta(\eta) = 1, at \quad \eta = 0 \tag{34}$$

$$F'(\eta) \leftrightarrow 0, G(\eta) \leftrightarrow 0, \theta(\eta) \to 0 \quad at \quad \eta \to \infty \tag{35}$$

The first sentences are given in terms of F and θ and G:

$$F_0(\eta) = \eta^3 - 4\eta^2 + \eta, \theta_0(\eta) = \eta + 2, G_0(\eta) = \eta + 3 \tag{36}$$

After working out the straight parts of the equations, we figure out what λ_1, λ_2, and λ_3 are by doing some calculations:

$$\lambda_1 = \frac{1}{8}(\tau - \eta)^3 \tag{37}$$

$$\lambda_2 = \tau - \eta \tag{38}$$

$$\lambda_3 = \tau - \eta \tag{39}$$

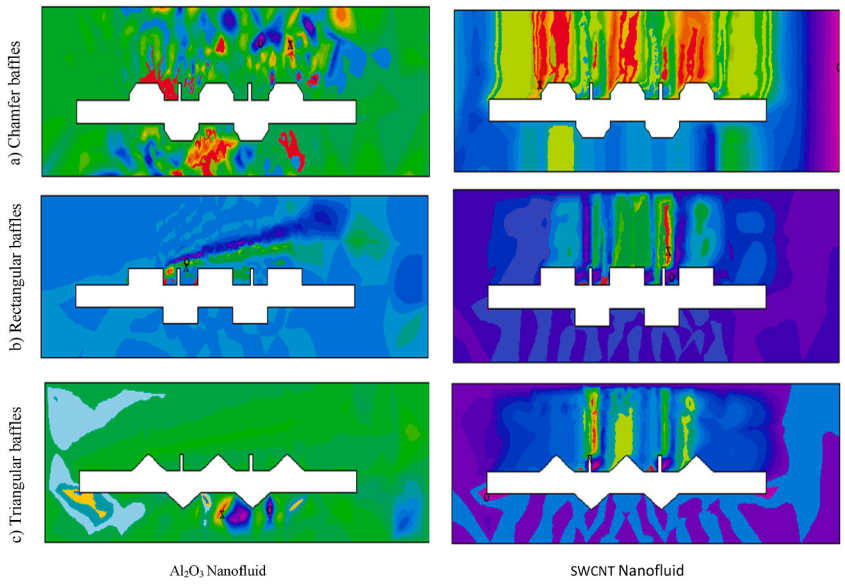

Fig. 7. Spreading angular velocity from different types of blades with different geometries with two nanofluids SWCNT and Al_2O_3.

$$F_1(\eta)=\eta^4-4\eta^2+3\eta+\frac{1}{4}\left(-\frac{1}{8}R\left((4\eta^2-2\eta+1)(6\eta-3)-(3\eta^3-2\eta^2+\eta)(8\eta-4)\right)-\frac{1}{8}M(6\eta-3)\right)\eta^4 \\ -\frac{1}{24}\eta^4\left(-R\left((3\eta^4-2\eta+1)(6\eta-3)-(4\eta^3-2\eta^4+\eta)(6\eta-3)\right)-M(6\eta-3)\right) \tag{36}$$

$$\theta_1(\eta)=-3\eta+2-\frac{1}{8}\left(-Pr\varnothing\left(2\eta^3-4\eta^2+\eta\right)+\varnothing\right)\eta^2 \tag{40}$$

$$G_1(\eta)=-\eta+3+\frac{1}{8}Pr.\,R\left(3\eta^3-2\eta^4+\eta\right)\eta^3 \tag{41}$$

Finally, by summing up the sentences at Pr = 3, M = 0, S = 0, and α = 1:

$$F(\eta)=F_1(\eta)\rightarrow F(\eta)=\eta^4-4\eta^2+3\eta+\frac{22}{12}\eta^8-\frac{32}{12}\eta^7+\frac{5}{3}\eta^6-\frac{2}{3}\eta^5-\frac{2}{4}\eta^4 \tag{42}$$

$$\theta(\eta)=(\eta+0.9643)\times(\eta-0.7203)\times(\eta-1.6540)\times\left(\eta^4-0.4654\right)\times(\eta+0.7753) \tag{43}$$

$$G(\eta)=G_1(\eta)\rightarrow G(\eta)=0.8(\eta+1.7029)\times(\eta-3)\times(\eta-2.5558)\times\left(\eta^4-0.3260\right)\times\left(\eta+541\right) \tag{44}$$

4. Results and discussion

This hybrid section compared the effects of Al_2O_3 and SWCNT nanoparticles on tilted, rectangular, and triangular ribs. With the analytical and numerical method of Vim, the parameters of dimensionless couple equations have been investigated and calculated at first. The volume concentration of nanofluids is between 0.03 and 0.04. The evaluations and results obtained from the VIM method have been carried out in Maple International software. Figure (4a) demonstrates how fast something spins when injected onto a stretched surface. The equations act differently if we make the magnetic parameter smaller and don't change anything else. Furthermore, it can be observed from Figures (4b-5) that the stream function tends towards a constant value after reaching a specific deal of η. The application of semi-analytical methods in this study resulted in highly accurate outcomes, and the convergence of solutions was notably apparent. The impact of the magnetic parameter on the velocity field for suction and injection on a stretching sheet is depicted in Figure (5). As a result of the magnetic parameter's presence, an increase in thermal boundary layer thickness is demonstrated.

Figure (6) shows the temperature change of the nanoliquid emanating from the stretch sheet. A comparison between two nanofluids moving from different dimensions of the stretching plate has been obtained, shown in the following graphs. In the position of the chamfer-shaped blades, due to the use of two nanofluids, the result is that the thermal range and the amount of heat transfer between the SWCNT nanotube and the plate are higher than that of aluminum oxide and the sheet. The temperature in the vicinity of the triangular baffles is 39°, whereas an elevated temperature of aluminum oxide is observed near the rectangular and chamfer baffles. Additionally, the temperature of aluminum oxide decreases from the surface towards the upper region. The temperature and heat transfer values around the baffles are 26° and 30°, respectively. When the nanofluid of aluminum oxide bypasses the baffles, the

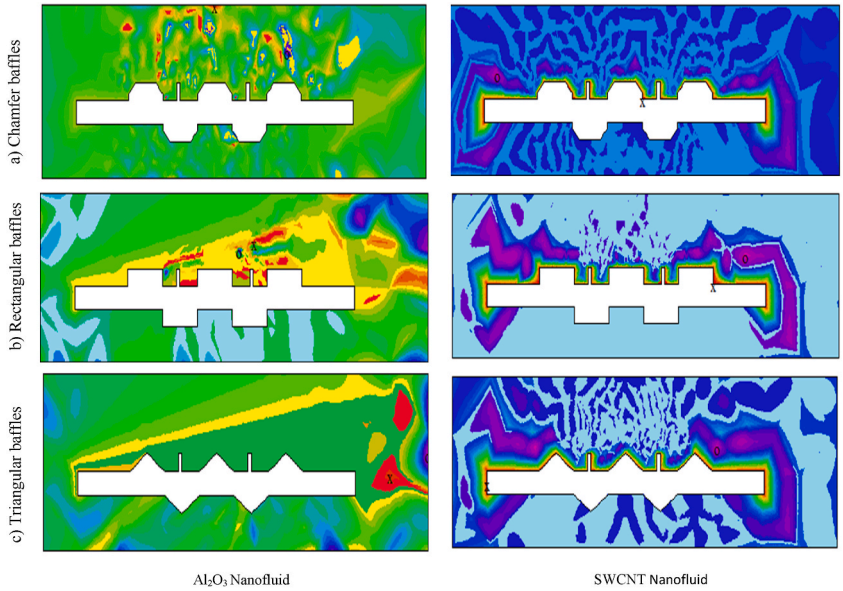

Fig. 8. Spreading angular velocity from different types of blades with different geometries with two nanofluids SWCNT and Al_2O_3.

Table 3
A different situation of the numerical value of the temperature parameter in the types of vanes installed on the tension sheet.

x	Chamfer baffles		Rectangular baffles		Triangular baffles	
	Al_2O_3	SWCNT	Al_2O_3	SWCNT	Al_2O_3	SWCNT
0.0	−6.6	22.78	21.09	22.34	26.44	22.15
0.1	8.13	27.47	20.11	29.32	29.88	27.17
0.2	29.98	30.44	29.03	29.76	29.36	29.99
0.5	19.23	29.77	32.09	29.12	29.72	29.00
0.8	7.45	28.19	27.40	28.94	28.32	28.81
0.9	−2.04	16.01	27.83	17.21	27.90	16.54
1.0	13.21	22.33	22.35	21.70	23.00	21.64

temperature rises to 28° while the heat transfer value remains at 30°. When SWCNT nanofluid flows over the stretching surfaces, the temperature around various baffles is high, and space baffles have an elevated temperature. The temperature of SWCNT has a maximum value around the baffles and blades, but it decreases as it bypasses from the surface towards the top. The average temperature of SWCNT nanofluid near the baffles is 30°. Upon comparing the SWCNT and Al_2O_3 nanofluids flow over different baffles and blades, the findings indicate that the temperature of SWCNT nanofluid around the baffles is higher than that of Al_2O_3 nanofluids. As can be seen in the figure below, in the vicinity of the surface of the sheet and in the state of passage of the SWCNT nanofluid, it has its maximum heat and heat transfer values, and at this time the thermal boundary layer will have a large thickness. The thermal boundary layer in this case has a larger and larger range than the case of aluminum oxide nanofluid passage.

Fig (7) shows how the velocity of tiny particles in fluids changes when they move across a surface that is being stretched. When aluminum oxide moves through triangular or chamfer baffles with two blades, its average velocity is 2.5 m per second. The chamfer baffles' highest spinning velocity below the stretching surface is 4.50 m per second. The velocity at which the two blades in the flat baffles move around is slow. But, when we pour small fluid through the top of the baffles, the velocity of the blades goes up. When tiny particles called SWCNT go over a flat sheet being pulled, they spin fast around some small square shapes. This thing is spinning fast at 4–5 m per second. When baffles have two blades and are either triangular or rectangular, the velocity of the air around them is smooth and not too fast. But near the edges of the blades and baffles, the air moves faster, reaching velocities between 3 and 4.5 m per second. When we looked at how SWCNT and Al_2O_3 nanofluids moved over the edges of baffles and blades, we found that Al2O3 moved faster than Al_2O_3 Nanoparticles. The spinning of triangular parts in Al_2O_3 nanoparticles is faster than in SWCNT nanoparticles.

This picture (Fig. 8) shows how fast nanofluids move when they flow over a surface that is being stretched. The Al_2O_3 nanofluid is quicker than SWCNT near the edges and surface, as shown in Figure (a-8). The velocity of aluminum oxide is usually around 1.30 m per second. The fastest velocity of the SWCNT nanofluid happens close to the baffles and surface, and it's 35 (m/s). The same rules apply to other baffles and blades in small SWCNT fluid. The slowest velocity of Al_2O_3 nanofluid happens near the triangle-shaped parts on the bottom (c-8).

Based on the information in Table 3, the rectangular baffles have the highest heat transfer and temperature for Al_2O_3, with a difference of 0.14 compared to the triangular and chamfers baffles. The maximum temperature was 32.54 at x = 0.6, while the chamfer

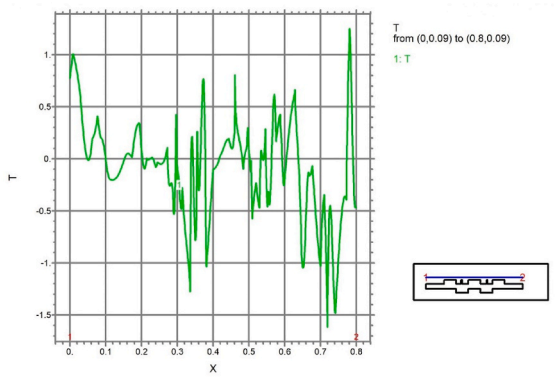

a. Two-dimensional diagram of temperature changes of aluminum oxide nanoparticles on oblong blades.

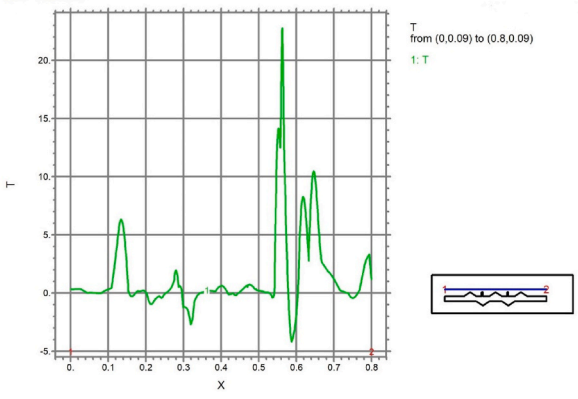

b. Two-dimensional diagram of temperature changes of aluminum oxide nanoparticles on triangular blades.

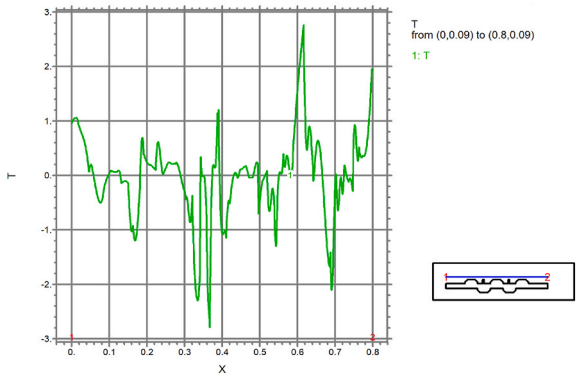

c. Two-dimensional diagram of temperature changes of aluminum oxide nanoparticles on chamfer blades.

Fig. 9. Two-dimensional diagram of temperature changes of aluminum oxide nanoparticles on chamfer, rectangular and triangular blades.

baffles had the lowest temperature for Al_2O_3 nanoparticles.

Based on Fig. 9, we have obtained temperature changes at different points of the sheet surface, which are represented on a two-dimensional diagram. It appears that the highest density of temperature lines occurs when oblong blades are used. In simpler terms, the temperature gradient between the initial and final points is larger when oblong blades are utilized compared to other blades. The conclusion taken from this diagram is that the larger the outer surface of the blade, the higher the heat exchange rate between the nanofluid and the temperature of the solid body.

In Fig. 10, the velocity changes of aluminum oxide nanofluid are depicted in three dimensions as it passes over rectangular, triangular, and chamfer-shaped blades. To put it in simpler terms, when using oblong shaped blades on a tensile sheet, the boundary layer with the highest thickness experiences the maximum velocity. This leads to an increase in the movement of aluminum oxide fluid

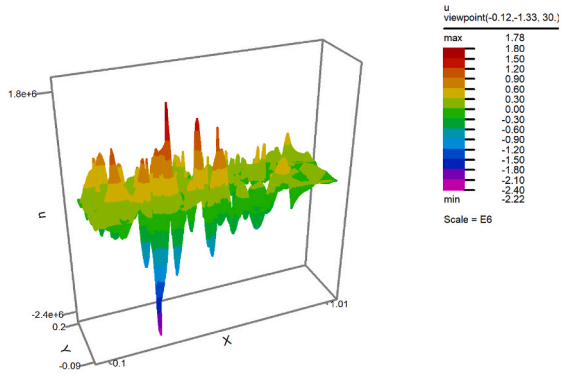

a. Three-dimensional diagram of velocity changes of aluminum oxide nanofluids on chamfer blades.

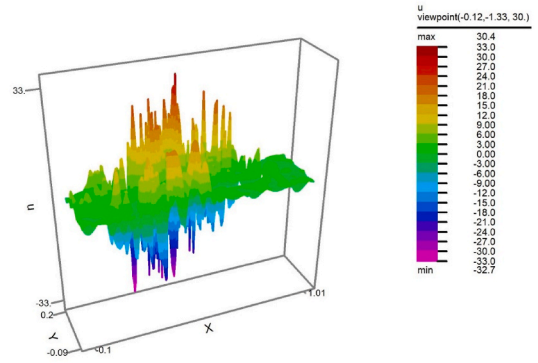

b. Three-dimensional diagram of velocity changes of aluminum oxide nanofluids on triangular blades.

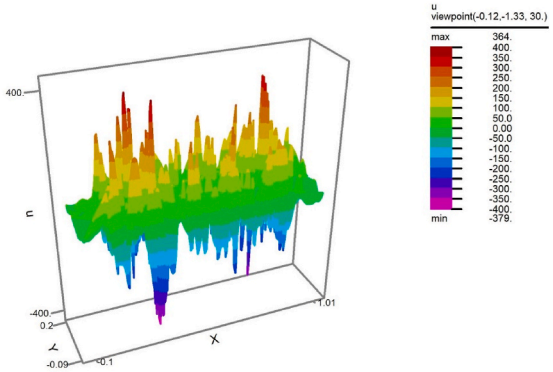

c. Three-dimensional diagram of velocity changes of aluminum oxide nanofluids on rectangular blades.

Fig. 10. Three-dimensional diagram of velocity changes of aluminum oxide nanofluid on chamfer, rectangular and triangular blades.

Table 4
A different situation of the numerical value of the velocity parameter in the types of vanes installed on the tension plate.

x	Chamfer baffles		Rectangular baffles		Triangular baffles	
	Al_2O_3	SWCNT	Al_2O_3	SWCNT	Al_2O_3	SWCNT
0.0	0.06	−0.20	0.47	0.39	0.46	0.39
0.1	0.50	0	0.73	−0.33	0.75	−0.48
0.2	1.19	−0.25	1.54	−0.29	1.21	0
0.5	−2.79	0.61	3.76	0	2.92	−0.19
0.7	2.33	−0.23	1.48	−0.38	2.78	−0.33
0.9	0.40	−0.19	2.33	−0.18	1.65	−0.20
1.0	0.88	0	−0.45	0	−1.70	0

Table 5
A different situation of the numerical value of the angular velocity parameter in the types of vanes installed on the tension plate.

x	Chamfer baffles		Rectangular baffles		Triangular baffles	
	Al_2O_3	SWCNT	Al_2O_3	SWCNT	Al_2O_3	SWCNT
0.0	0.42	0	0	28	−6.87	31
0.1	0.36	78	0	50	0.33	48
0.2	−0.43	118	0	68	4.78	62
0.5	0.27	0.05	1.58	53	4.98	44
0.8	−0.42	57	0.56	39	−2.87	39.8
0.9	−0.36	−47	−0.37	0	−6.8	0
1.0	0.05	−77	−0.32	0	4.99	0

molecules around the hot plate, resulting in a higher level of exchange between solid and liquid particles.

Table (4) indicates that the highest nanofluid velocity is observed near the rectangular baffles for Al_2O_3, with a difference of 0.19.4% compared to chamfer baffles and 0.12.23% compared to triangular baffles. The maximum velocity of 3.66 was recorded at x = 0.6, while the chamfer baffles demonstrated the lowest nanofluid velocity for Al_2O_3 nanoparticles.

Table (5) provides information on the nanofluid angular velocity, which shows that the highest value is found near the chamfer baffles for SWCNT, with a difference of 0.77% compared to rectangular baffles and 0.95% compared to triangular baffles. The maximum angular velocity was measured at x = 0.3, and the lowest value was recorded near the chamfer baffles for SWCNT nanoparticles at x = 0.9.

The next part discusses how Design-Expert software uses the Response Surface Methodology. This essay studied how to improve the flow and thermal process of a nanofluid passing over a stretched sheet using the Response Surface Methodology. Response Surface Methodology, or RSM for short, is a set of statistical techniques and applied mathematics for constructing experimental models. Response surface designs aim to optimize the response (output variable) affected by several independent variables (input variables). An experiment is a series of tests called execution. Fourteen tests were performed using a specialized technique in the Design-Expert software to achieve optimal results from the computer program. By analyzing two-dimensional diagrams based on fluid parameters such as baffle and blade height and the distance between baffles, we could identify the optimal points for nanofluid velocity, angular velocity, and equivalent liquid temperature.

Pictures 11(a) to 11(c) show how the actual results compare to what we expected for things like how fast the fluid is moving and how hot it is. Fig. 11 shows more test results in the experiment than in actual experiments. However, the real-life temperatures have a higher average when looking at the temperature readings. Figure (11) shows that our Response Surface Methodology test is accurate because it primarily uses natural, not laboratory, values. The balance line is the middle line in 12–14 shapes. It helps compare actual and laboratory data. As a result of the curve's linearity and the proximity of data points to each other, this experiment can be considered valid. The difference between the actual and experimental results is minimal, indicating a low error rate.

Fig. 12 explores the velocity of nanofluid across varying changes in baffle height (ranging from 0.03 to 0.068) and distances between baffles (ranging from 0.04 to 0.06). The simulation shows the maximum and minimum nanofluid velocity, with the highest velocity occurring when the baffle height is at 0.059, and the distance between baffles is at 0.06. It was observed that as the distance between baffles increased, the velocity of the nanofluid also increased. Figure (13) examines the temperature of the nanofluid, with varying changes in baffle height (between 0.04 and 0.06) and distances between baffles (ranging from 0.05 to 0.07). The simulation shows the maximum and minimum temperatures for the nanofluid, with the highest temperature occurring when the baffle height is at 0.06, and the distance between baffles is at 0.07. It was observed that there is a positive correlation between the length of baffles and the velocity of nanofluid, with an increase in the distance increasing velocity. On the other hand, the minimum temperature for the nanofluid was recorded when the baffle height was at 0.055, and the distance between baffles was at 0.06. At this point, the temperature of the nanofluid was noted to be 17°.

Figure (14) investigates the nanofluid temperature across different changes in blade height (ranging from 0.04 to 0.06) and distances between baffles (ranging from 0.05 to 0.07). The simulation shows the maximum and minimum temperatures for the nanofluid. As per the simulation results, the highest temperature for the nanofluid was recorded when the blade height was at 0.061, and the distance between baffles was at 0.068. The temperature of the nanofluid was noted to increase with an increase in the space between baffles. Alternatively, the minimum temperature for the nanofluid was documented when the blade height was at 0.042, and the distance between baffles was at 0.056. The temperature of the nanofluid was measured to be 17°.

The 2D temperature cantor in Figure (15) displays how changes in the blade height to baffle height ratio affect the temperature of the nanofluid. The results show that increasing blade height resulted in an increase in nanofluid temperature from T = 19 to T = 23. It was interpreted that using longer blades on the stretching sheet promotes better heat transfer due to the heat convection being sufficient and fluid pressure being high in this mode.

Figure (16) investigates the angular velocity of the nanofluid by analyzing changes in baffle height (ranging from 0.04 to 0.06) and distance between baffles (ranging from 0.05 to 0.07). The simulation shows the maximum and minimum angular velocities of the nanofluid. The highest angular velocity was recorded when the baffle height was 0.07, and the distance between baffles was 0.068. Based on the simulation results, it was observed that there is a positive correlation between the distance of baffles and the angular velocity of the nanofluid, with an increase in the length leading to an increase in velocity. The lowest angular velocity for the nanofluid was recorded when the baffle height was at 0.053 and the distance between baffles was at 0.06. At this point, the velocity of the

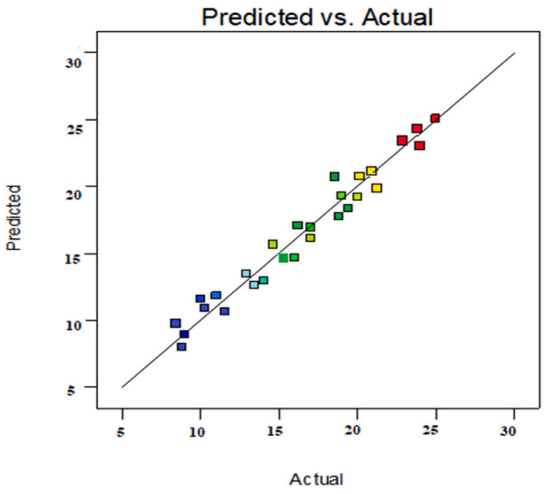

(a)

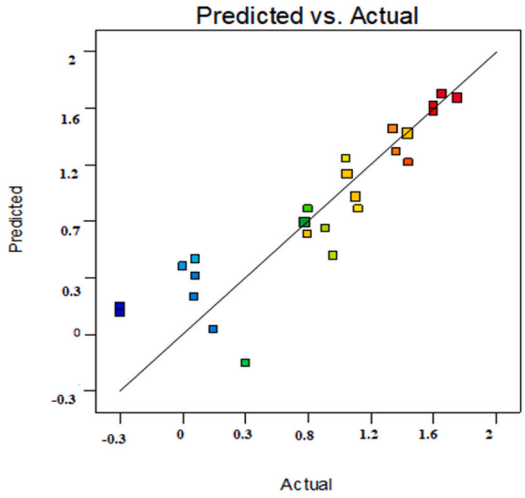

(b)

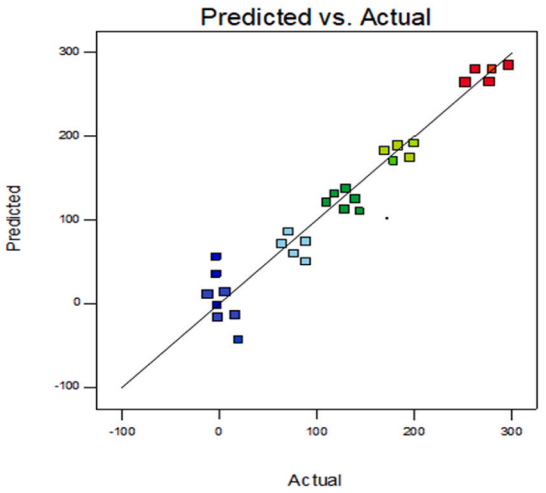

Fig. 11. A statistical chart showing predictable data with actual values for temperature, velocity and angular velocity.

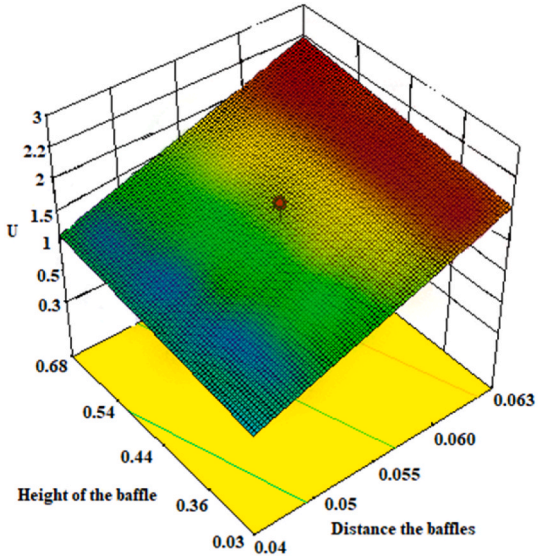

Fig. 12. Three-dimensional graph of the velocity gradient in the conditions of placement of the blades with respect to certain distances relative to each other with the RSM technique.

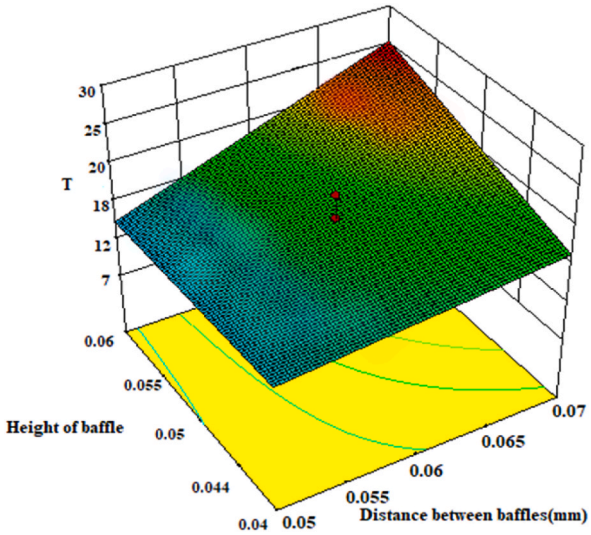

Fig. 13. Three-dimensional graph of the velocity gradient in the conditions of placement of the blades with respect to certain distances relative to each other with the RSM technique.

nanofluid was measured to be 0.014 m/s.

Figure (17) studies the angular velocity of the nanofluid, analyzing changes in blade height (ranging from 0.030 to 0.045) and distance between baffles (ranging from 0.05 to 0.07). The simulation aims to identify the nanofluids maximum and minimum angular velocities. Based on the simulation results, the highest angular velocity for the nanofluid was recorded when the blade height was at 0.033 and the distance between baffles was at 0.051. It was noticed that there is a positive correlation between the distance of baffles and the angular velocity of the nanofluid, with an increase in the distance increasing velocity. The lowest angular velocity for the nanofluid was documented when the baffle height was at 0.030 and the distance between baffles was at 0.057. At this point, the velocity of the nanofluid was observed to be 0.014 m/s. Furthermore, it was noted that by increasing the blades' height, the nanofluids angular velocity also increased.

Figure (18) displays the 2D angular velocity cantor, which examines the effect of changes in the blade height to baffle height ratio on the angular velocity of the nanofluid. The simulation results show that increasing the blade height increased velocity from N = 80 to N = 1330. It was interpreted that using longer blades on the stretching sheet promotes a faster fluid cycle due to the heat convection being sufficient and fluid pressure being high in this mode. According to the results from the graphs of how fast something is turning and the factors that transfer heat in the software called Design-Expert, the best improvement happened when the velocity and

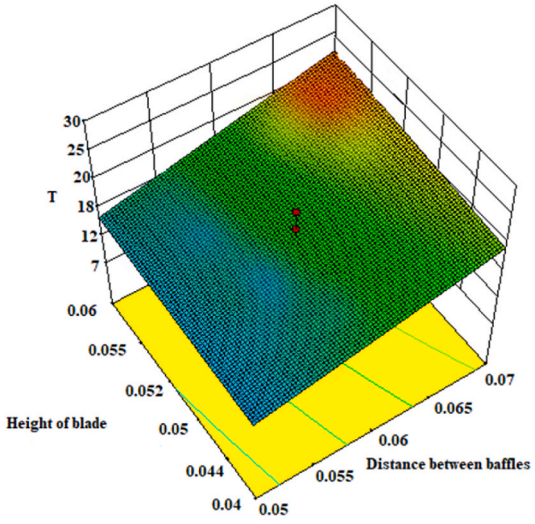

Fig. 14. Three-dimensional graph of the temperature gradient in the conditions of placement of the baffles with respect to certain distances relative to each other with the RSM method.

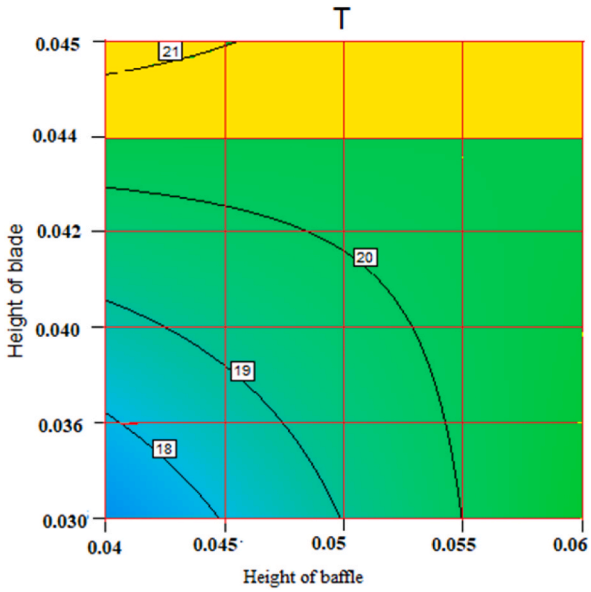

Fig. 15. A view of the two-dimensional space of the temperature gradient of nanoparticles according to the height of the blades and vanes within the scope of the RSM statistical method.

temperature of the small particles in the liquid were at u = 1.12 and T = 20.18, and the turning velocity was N = 137.29 The general specifications are determined in the following way:

The distance between baffles is 0.071 units, the height of baffles are 0.059 units, the height of blades are 0.037 units, the value of u is 1.12, the value of T is 20.18, and the value of N is 137.29.

5. Conclusion

This paper explores how the temperature and velocity change in a specific direction and the rotational velocity when nanofluids flow through triangular, rectangular, and chamfer fins. The study also takes into account the presence of a consistent magnetic field. The new initiative used in this study includes the parameters of SWCNT and Al2O3 nanoparticles that pass through different baffles and blades, and the results obtained from them are compared.

Also, optimizing heat transfer parameters and angular velocity of nanoparticles is done using the Response Surface Methodology (RSM) method. The Finite Element Method is chosen to solve the main equations. The second part of the explanation is about how the

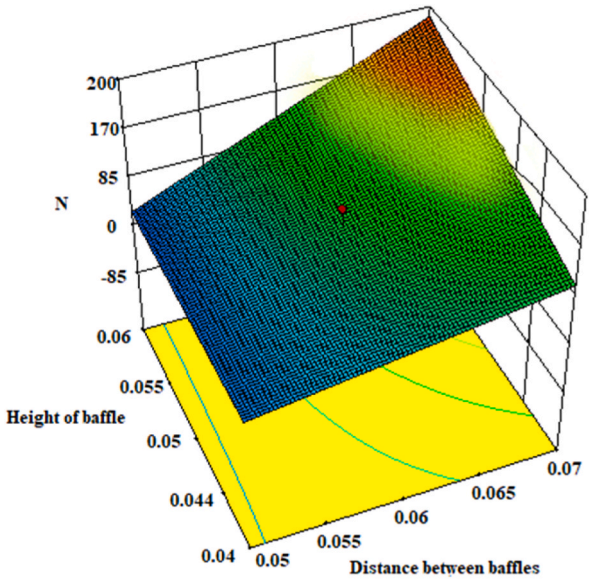

Fig. 16. Three-dimensional graph of the angular velocity gradient in the conditions of placement of the blades with respect to certain distances relative to each other with the RSM technique.

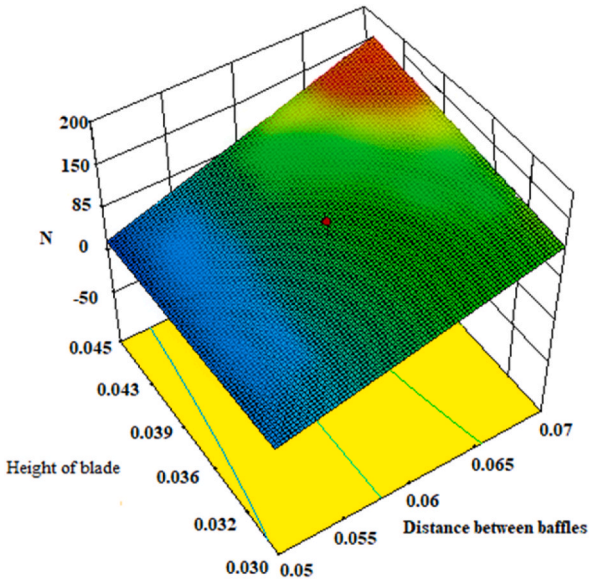

Fig. 17. Three-dimensional graph of the angular velocity gradient in the conditions of placement of the baffles with respect to certain distances relative to each other with the RSM method.

Design-Expert software uses the Response Surface Methodology. This paper utilized the RSM method to optimize the velocity of nanofluid and heat transfer as it passes through the stretching sheet. The significance of this research lies in identifying the more efficient and economically viable type of nanofluid for industrial use by comparing the two types. Additionally, the RSM method was employed to determine the appropriate distance between and diameter of the blades to heat the plate and fluid effectively. The utilization of two SWCNT and Al2O3 nanofluids in this study was due to their superior conduction heat transfer coefficient and ability to transfer heat efficiently at a constant pressure.

- To summarize, after analyzing the flow of SWCNT and Al_2O_3 nanofluids on various baffles and blades, it was found that the temperature of SWCNT nanofluid around the baffles was higher compared to the temperature of Al_2O_3 nanofluids.
- Simply put, the velocity of Aluminum oxide nanofluid is higher than that of SWCNT in the chamfer baffles and surface area. The average velocity of Aluminum oxide nanofluid is measured at 1.20 (m/s), while the highest velocity of SWCNT nanofluid is recorded near the baffles and surface, with a velocity rate of 33 (m/s).

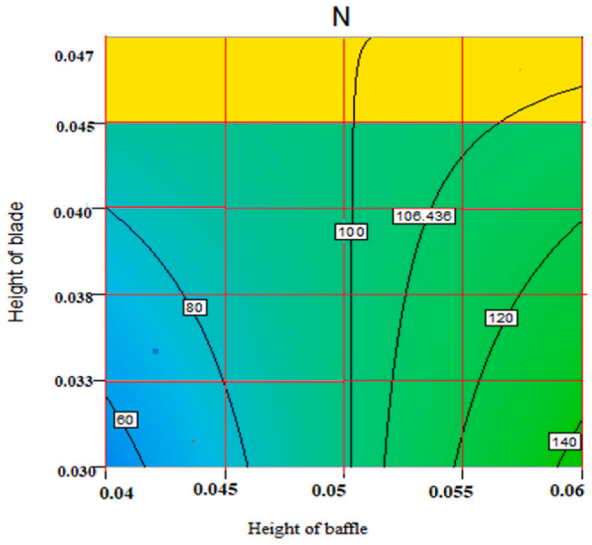

Fig. 18. A view of the two-dimensional space of the angular velocity gradient of nanoparticles according to the height of the blades and vanes within the scope of the RSM statistical method.

- According to the results from the graphs of how fast something is turning and the factors that transfer heat in the software called Design-Expert, the best improvement happened when the velocity and temperature of the small particles in the liquid were at u = 1.12 and T = 20.18, and the turning velocity was N = 137.29.

Authorship contributions

Bashar Mahmood Ali: Wrote the paper and Contributed analysis tools or data.
As'ad Alizadeh: Conceived and designed the analysis.
Kadhim Abbas Jabbar: Analyzed and interpreted the data.
Ahmed hasoon: Conceived and designed the analysis.
Mahmoud Shamsborhan: Contributed analysis tools or data.
Pooya Pasha: Analyzed and interpreted the data Wrote the paper.

Declaration of competing interest

The authors declare that they have no known competing financial interests or personal relationships that could have appeared to influence the work reported in this paper, This article has no funding from the university or any institution.

Data availability

The data that has been used is confidential.

References

[1] P. Pasha, S. Mirzaei, M. Zarinfar, Application of numerical methods in micropolar fluid flow and heat transfer in permeable plates, Alex. Eng. J. 61 (2021) 2663–2672.
[2] Fatemeh Yousefi, et al., UV-shielding properties of a cost-effective hybrid PMMA-based thin film coatings using TiO2 and ZnO nanoparticles: a comprehensive evaluation, Sci. Rep. 13 (1) (2023) 7116.
[3] Meisam Ashrafivala, et al., Investigation of H2O2/UV advanced oxidation process on the removal rate of coliforms from the industrial effluent: a pilot-scale study, Int. J. Hydrogen Energy 47 (78) (2022) 33530–33540.
[4] Seyed Borhan Mousavi, Saeed Zeinali Heris, Experimental investigation of ZnO nanoparticles effects on thermophysical and tribological properties of diesel oilInt, J. Hydrogen Energy 4543 (2020) 23603–23614.
[5] Seyed Borhan Mousavi, Zeinali Heris Saeed, Mir Ghasem Hosseini, Experimental investigation of MoS2/diesel oil nanofluid thermophysical and rheological properties, Int. Commun. Heat Mass Tran. 108 (2019), 104298.
[6] Ferdosi, Sima Besharat, Thermal effect on the post-buckling and mechanical response of single-walled carbon nanotubes: a numerical investigation, J. Inst. Eng. 9 (2022) 1–6.
[7] Weiqi Zhao, et al., Synthesis of a functionalized carbon nanotube graphene composite enabling pH-responsive electrochemical sensing for biomedical applications, ACS Appl. Electron. Mater. 52 (2023) 1224–1233.
[8] Somayeh Sepahvand, Mostafa Bahrami, Narges Fallah, Photocatalytic degradation of 2, 4-DNT in simulated wastewater by magnetic CoFe2O4/SiO2/TiO2 nanoparticles, Environ. Sci. Pollut. Control Ser. 29 (5) (2022), 64796490.
[9] Amirhosein Mosavi, et al., Analysis of entropy generation of ferrofluid flow in the microchannel with twisted porous ribs: the two-phase investigation with various porous layers, Powder Technol. 380 (2021) 349–357.

[10] Masih Shekaramiz, et al., MHD nanofluid free convection inside the wavy triangular cavity considering periodic temperature boundary condition and velocity slip mechanisms, Int. J. Therm. Sci. 170 (2021), 107179.
[11] Pouyan Talebizadehsardari, et al., An experimental investigation for study the rheological behavior of water–carbon nanotube/magnetite nanofluid subjected to a magnetic field, Phys. Stat. Mech. Appl. 534 (2019), 122129.
[12] Jian-Feng Zhong, et al., Investigation of Ferro-nanofluid flow within a porous ribbed microchannel heat sink using single-phase and two-phase approaches in the presence of constant magnetic field, Powder Technol. 387 (2021) 251–260.
[13] Mahmoud Behrouz, et al., Mass-based hybridity model for thermomicropolar binary nanofluid flow: first derivation of angular momentum equation, Chin. J. Phys. 83 (2023) 165–184.
[14] Saeed Dinarvand, et al., Squeezing flow of aqueous CNTs-Fe3O4 hybrid nanofluid through mass-based approach: effect of heat source/sink, nanoparticle shape, and an oblique magnetic field, Results Eng. 17 (2023), 100976.
[15] Hamza Berrehal, Saeed Dinarvand, Ilyas Khan, Mass-based hybrid nanofluid model for entropy generation analysis of flow upon a convectively-warmed moving wedge, Chin. J. Phys. 77 (2022) 2603–2616. .
[16] Mohammad Izady, et al., Flow of aqueous Fe2O3–CuO hybrid nanofluid over a permeable stretching/shrinking wedge: a development on Falkner–Skan problem, Chin. J. Phys. 74 (2021) 406–420. .
[17] Emad Ismat Ghandourah, et al., Performance assessment of a novel solar distiller with a double slope basin covered by coated wick with lanthanum cobalt oxide nanoparticles, Case Stud. Therm. Eng. 32 (2022), 101859.
[18] Pham Van Vinh, Nguyen Van Chinh, Abdelouahed Tounsi, Static bending and buckling analysis of bi-directional functionally graded porous plates using an improved first-order shear deformation theory and FEM, Eur. J. Mech. Solid. 96 (2022), 104743. .
[19] Ibham Veza, et al., Response surface methodology (RSM) for optimizing engine performance and emissions fueled with biofuel: review of RSM for sustainability energy transition, Results in Engineering (2023), 101213.
[20] Hui-Lane Lau, et al., Optimization of fermentation medium components by response surface methodology (RSM) and artificial neural network hybrid with genetic algorithm (ANN-GA) for lipase production by Burkholderia cenocepacia ST8 using used automotive engine oil as substrate, Biocatal. Agric. Biotechnol. 50 (2023), 102696.
[21] Sandeep Gunalan, et al., Microwave-assisted extraction of biomolecules from moringa (Moringa oleifera Lam.) leaves var. PKM 1: a optimization study by response surface methodology (RSM), Kuwait J. Sci. 50 (2023) 339–344.
[22] H.C. Brinkman, The viscosity of concentrated suspensions and solutions, J. Chem. Phys. 20 (4) (1952), 571-571.
[23] B. Jalili, S. Sadighi, P. Jalili, D.D. Ganji, Characteristics of ferrofluid flow over a stretching sheet with suction and injection, Case Stud. Therm. Eng. 14 (2019), 100470.
[24] G.C. Bourantas, V.C. Loukopoulos, MHD natural-convection flow in an inclined square enclosure filled with a micropolar-nanofluid, Int. J. Heat Mass Tran. 79 (2014) 930–944.
[25] Paria Shadman, et al., Combined septum and chamfer fins on threated stretching surface under the influence of nanofluid and the magnetic parameters for rotary seals in computer hardware, Alex. Eng. J. 62 (2023) 489–507. .
[26] U. Khan, N. Ahmed, S.T. Mohyud-Din, Numerical investigation for three dimensional squeezing flow of nanofluid in a rotating channel with lower stretching wall Suspended by carbon nanotubes, Appl. Therm. Eng. 113 (2017) 1107–1117.
[27] K. Vajravelu, Viscous flow over a nonlinearly stretching sheet, Appl. Math. Comput. 124 (3) (2001) 281–288. .
[28] P. Pasha, D. Domiri-Ganji, Hybrid analysis of micropolar ethylene-glycol nanofluid on stretching surface mounted triangular, rectangular and chamfer fins by FEM strategy and optimization with RSM method, Int. J. Eng. 35 (5) (2022) 845–854. .
[29] Saeed Zeinali Heris, et al., Preparation and characterizations of TiO2/ZnO nanohybrid and its application in photocatalytic degradation of tetracycline in wastewater, J. Photochem. Photobiol. Chem. (2023), 114893.
[30] Shadi Bolouki Far, et al., Optimizing the amount of concentration and temperature of substances undergoing chemical reaction using response surface methodology, International Journal of Thermofluids 17 (2023), 100270.
[31] Marzieh Karimzadeh, et al., Heat transmission and magnetic effects on a ferrofluid liquid in a hybrid survey under the influence of two Helmholtz coils, Results in Engineering 16 (2022), 100702.
[32] Yuan Zhou, et al., Computational fluid dynamics and multi-objective response surface methodology optimization of perforated-finned heat sinks, J. Taiwan Inst. Chem. Eng. 145 (2023), 104823. .
[33] Jincheng Zhou, et al., Numerical study of mixed convection flow of two-phase nanofluid in a two-dimensional cavity with the presence of a magnetic field by changing the height of obstacles with artificial intelligence: investigation of entropy production changes and Bejan number, Eng. Anal. Bound. Elem. 148 (2023) 52–61. .
[34] Hadi Bordbar, et al., Flame detection by heat from the infrared spectrum: optimization and sensitivity analysis, Fire Saf. J. 133 (2022), 103673.
[35] Saeed Dinarvand, et al., MHD flow of MgO-Ag/water hybrid nanofluid past a moving slim needle considering dual solutions: an applicable model for hot-wire anemometer analysis, Int. J. Numer. Methods Heat Fluid Flow 32 (2) (2022) 488–510. .
[36] Saeed Dinarvand, et al., Squeezing flow of aqueous CNTs-Fe3O4 hybrid nanofluid through mass-based approach: effect of heat source/sink, nanoparticle shape, and an oblique magnetic field, Results in Engineering 17 (2023), 100976.
[37] Saeed Dinarvand, Nejad Alireza Mahdavi, Off-centered stagnation point flow of an experimental-based hybrid nanofluid impinging to a spinning disk with low to high non-alignments, Int. J. Numer. Methods Heat Fluid Flow 32 (8) (2021) 2799–2818. .